# Toward a generalized plate motion reference frame: Supplementary material

T. W. Becker

University of Southern California, Los Angeles CA, USA

A. J. Schaeffer

S. Lebedev

Dublin Institute of Advanced Studies, Dublin, Ireland

C. P. Conrad

University of Hawaii at Manoa, Honolulu HI, USA

## 1. Additional figures

We here provide four additional figures to complement the analysis discussed in the main text. Figure S1 shows the geographic distribution of misfit as a function of Euler pole location given fixed rotation amplitude (as obtained from the simplex inversions) for

---

T. W. Becker, Department of Earth Sciences, University of Southern California, 3651 Trousdale Pkwy., MC0740, Los Angeles CA 90089-0740, USA. (twb@usc.edu)

all models considered. See Table 1 of the main text; uncertainty ranges in Figure 2 of the main text were derived from the misfit metrics shown in the maps of Figure S1.

Figure S2a shows the orientational misfit within oceanic regions for the best-fit, spreading-aligned absolute plate motion (APM) model with azimuthal anisotropy from *Schaeffer and Lebedev* [2013a, b] at 150 km. Figure S2b shows the orientational misfit when the APM model is optimized to match seismic anisotropy itself.

Figure S3 repeats this analysis for orientational misfit for the model of *Debayle and Ricard* [2013] at 150 km, when compared to the spreading-aligned APM model and with the reference frame from optimizing against azimuthal from *Debayle and Ricard* [2013]. Figure S4 again repeats the analysis in the analogous way for the seismological model by *Yuan and Beghein* [2013].

A comparison of anisotropy with other models including lattice preferred orientation of olivine texture from actual mantle flow computations is discussed in *Becker et al.* [2014].

## References

Becker, T. W., C. P. Conrad, A. J. Schaeffer, and S. Lebedev (2014), Origin of azimuthal seismic anisotropy in oceanic plates and mantle, *Earth Planet. Sci. Lett.*, *401*, 236–250.

Debayle, E., and Y. Ricard (2013), Seismic observations of large-scale deformation at the bottom of fast-moving plates, *Earth Planet. Sci. Lett.*, *376*, 165–177.

Heuret, A., and S. Lallemand (2005), Slab dynamics and back-arc deformation, *Phys. Earth Planet. Inter.*, *149*, 31–51.

Morgan, W. J., and J. Phipps Morgan (2007), Plate velocities in the hotspot reference frame, in *Plates, Plumes, and Planetary Processes*, *Special Papers*, vol. 430, edited by

J. R. Foulger and D. M. Jurdy, pp. 65–78, Geological Society of America, Boulder, CO.

Schaeffer, A., and S. Lebedev (2013a), Global variations in azimuthal anisotropy of the Earth's upper mantle and crust (abstract), *Eos Trans. AGU*, pp. DI11A–2172, AGU Fall Meeting Abstract volume.

Schaeffer, A., and S. Lebedev (2013b), Global shear speed structure of the upper mantle and transition zone, *Geophys. J. Int.*, *194*, 417–449.

Yuan, K., and C. Beghein (2013), Seismic anisotropy changes across upper mantle phase transitions, *Earth Planet. Sci. Lett.*, *374*, 132–144.

**Figure S1.** Distribution of mean, global misfit as a function of Euler pole location, at constant rotation rate, for all APM model optimizations considered, in global Hammer (fixed) and Lambert azimuthal equal area (adjusted for $\boldsymbol{\omega}_{bf}$) projections. Title states best fit Euler pole from the simplex optimization (longitude, latitude, rate; Figure 2 of the main text), legend shows original (no-net-rotation, NNR) and best-fit (APM) values of misfit metric (Table 1 of the main text). **a)** Spreading-alignment model using all points as in Figure 1 of the main text, misfit $\langle \Delta\alpha \rangle_r$. **b, c, d)** Same as a), but restricted to spreading center point pairs in the Atlantic, Pacific, and Indian ocean, respectively (subscripts $_{r-A}$, $_{r-P}$, and $_{r-I}$ for $\langle \Delta\alpha \rangle$). **e)** Ridge-no-motion reference frame, $\langle \Delta\alpha \rangle_r$. **f, g, h)** Match of APM with azimuthal anisotropy at 150 km depth from the models of *Schaeffer and Lebedev* [2013a] (*cf.* Figure S2), *Debayle and Ricard* [2013], and *Yuan and Beghein* [2013], respectively, in all oceanic regions, $\langle \Delta\alpha \rangle_o$. **i** and **j)** best fit to station-averaged $SKS$ splitting, and when smoothed over 5°, respectively, $\langle \Delta\alpha \rangle_{SKS}$. **k)** Fit of velocities to the hotspot tracks of *Morgan and Phipps Morgan* [2007], $\langle \Delta v \rangle_h$. **l)** trying to minimize trench motions from *Heuret and Lallemand* [2005], $\langle \Delta v \rangle_t$.

**Figure S2.** Azimuthal seismic anisotropy [SL2013SVA in cyan; from *Schaeffer and Lebedev*, 2013a] at 150 km depth compared to different APM models (green) in the oceanic plates, plotted on top of local angular misfit, $\Delta\alpha$ [as in *Becker et al.*, 2014, their Figure 2]. **a)** is for the spreading-aligned APM model, **b)** for a model that minimizes the misfit to seismic anisotropy itself (Table 1, Figure 2 of the main text). Legend in lower left states the global mean misfit, $\langle\Delta\alpha\rangle_o$, in all oceanic plate regions, and when weighting each oceanic basin evenly, $\langle\Delta\alpha\rangle_{op}$ [see *Becker et al.*, 2014].

**Figure S3.** Azimuthal seismic anisotropy (cyan) at 150 km depth compared to different APM models (green) with local angular misfit, $\Delta\alpha$, as background. **a)** is for the spreading-aligned APM model, **b)** for a model that minimizes the misfit to seismic anisotropy itself. Analogous to Figure S2, but for DR2012 by *Debayle and Ricard* [2013].

**Figure S4.** Azimuthal seismic anisotropy (cyan) at 150 km depth compared to different APM models (green) with local angular misfit, $\Delta\alpha$, as background. **a)** is for the spreading-aligned APM model, **b)** for a model that minimizes the misfit to seismic anisotropy itself. Analogous to Figures S2 and S3, but for YB13 by *Yuan and Beghein* [2013].

# Figure S1

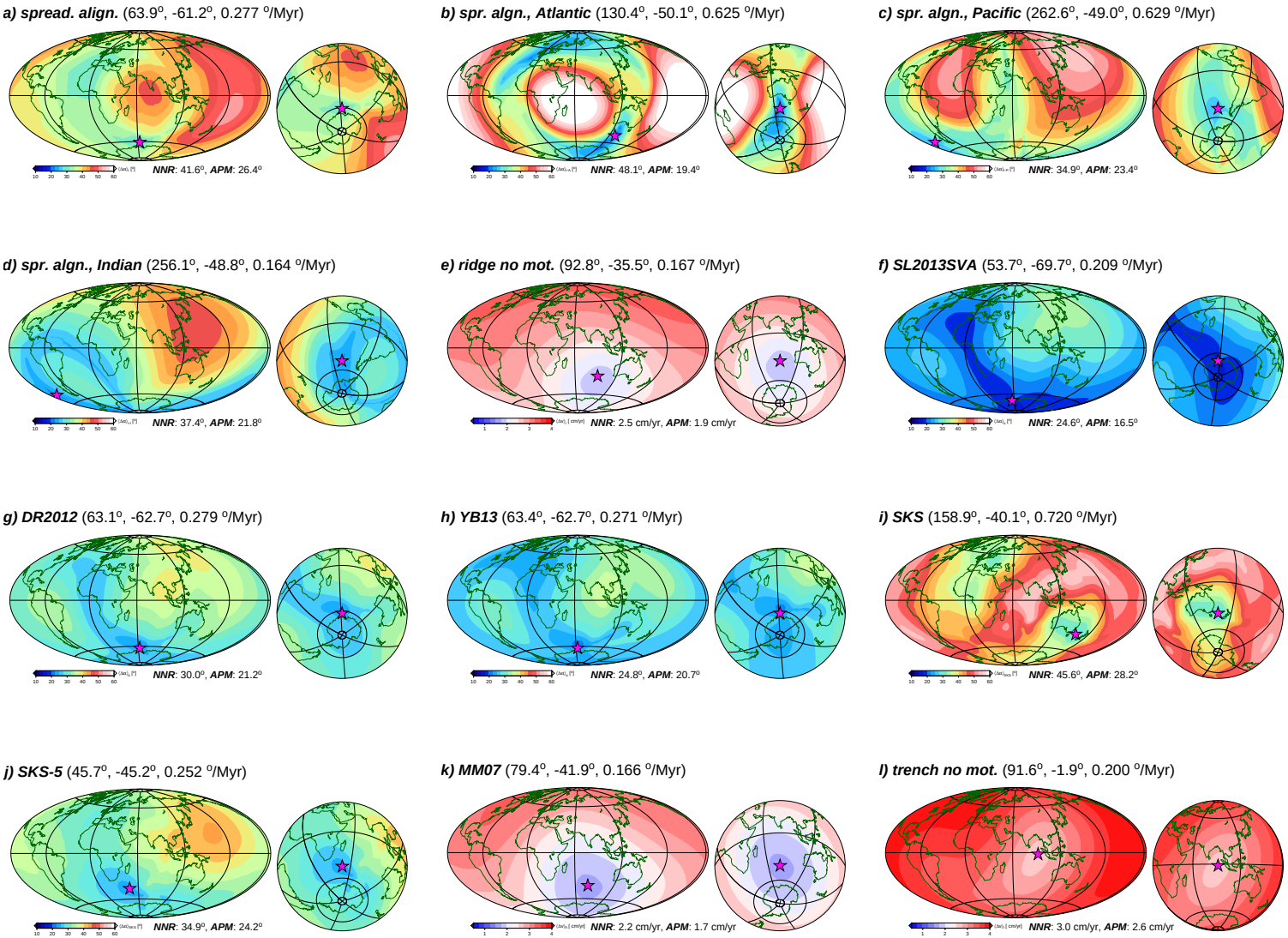
a) spread. align. (63.9°, -61.2°, 0.277 °/Myr)
NNR: 41.6°, APM: 26.4°
b) spr. algn., Atlantic (130.4°, -50.1°, 0.625 °/Myr)
NNR: 48.1°, APM: 19.4°
c) spr. algn., Pacific (262.6°, -49.0°, 0.629 °/Myr)
NNR: 34.9°, APM: 23.4°
d) spr. algn., Indian (256.1°, -48.8°, 0.164 °/Myr)
NNR: 37.4°, APM: 21.8°
e) ridge no mot. (92.8°, -35.5°, 0.167 °/Myr)
NNR: 2.5 cm/yr, APM: 1.9 cm/yr
f) SL2013SVA (53.7°, -69.7°, 0.209 °/Myr)
NNR: 24.6°, APM: 16.5°
g) DR2012 (63.1°, -62.7°, 0.279 °/Myr)
NNR: 30.0°, APM: 21.2°
h) YB13 (63.4°, -62.7°, 0.271 °/Myr)
NNR: 24.8°, APM: 20.7°
i) SKS (158.9°, -40.1°, 0.720 °/Myr)
NNR: 45.6°, APM: 28.2°
j) SKS-5 (45.7°, -45.2°, 0.252 °/Myr)
NNR: 34.9°, APM: 24.2°
k) MM07 (79.4°, -41.9°, 0.166 °/Myr)
NNR: 2.2 cm/yr, APM: 1.7 cm/yr
l) trench no mot. (91.6°, -1.9°, 0.200 °/Myr)
NNR: 3.0 cm/yr, APM: 2.6 cm/yr

***a) spread. align.***

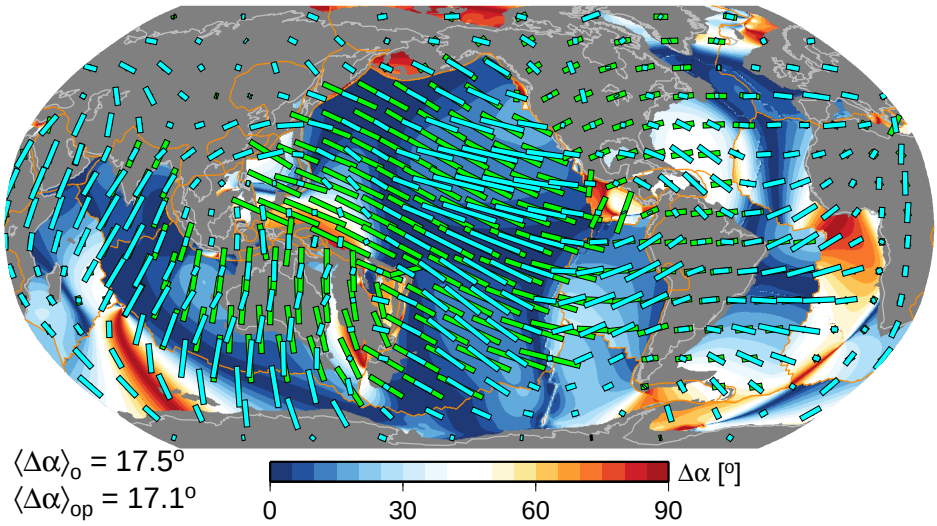


***b) SL2013SVA***

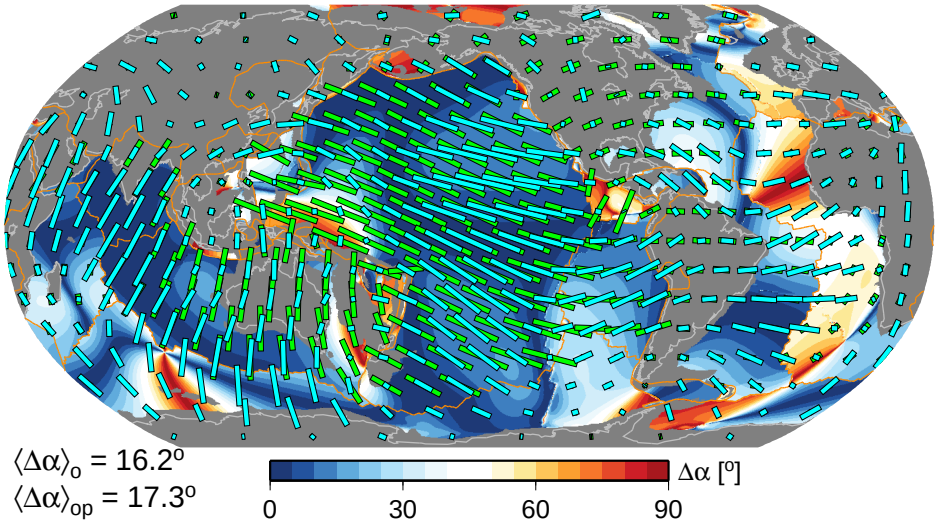


**Figure S2**

***a) spread. align.***

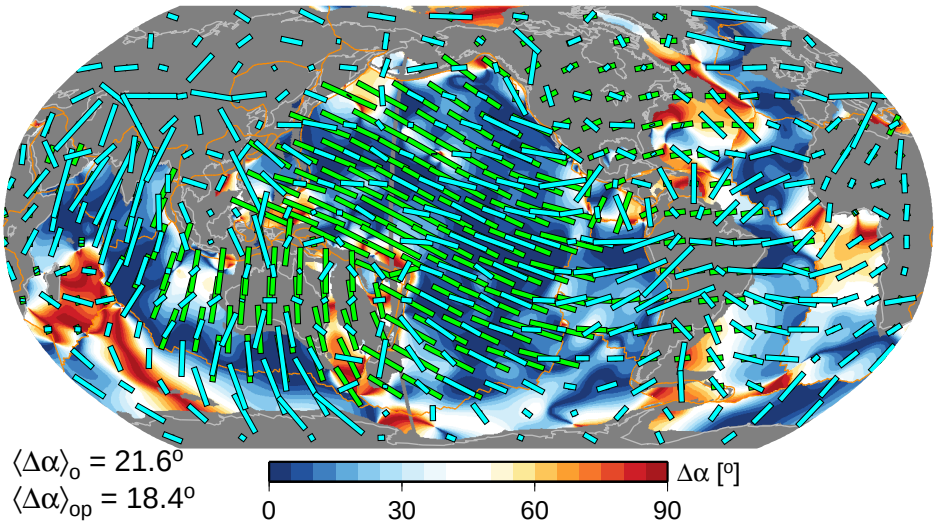


***b) DR2012***

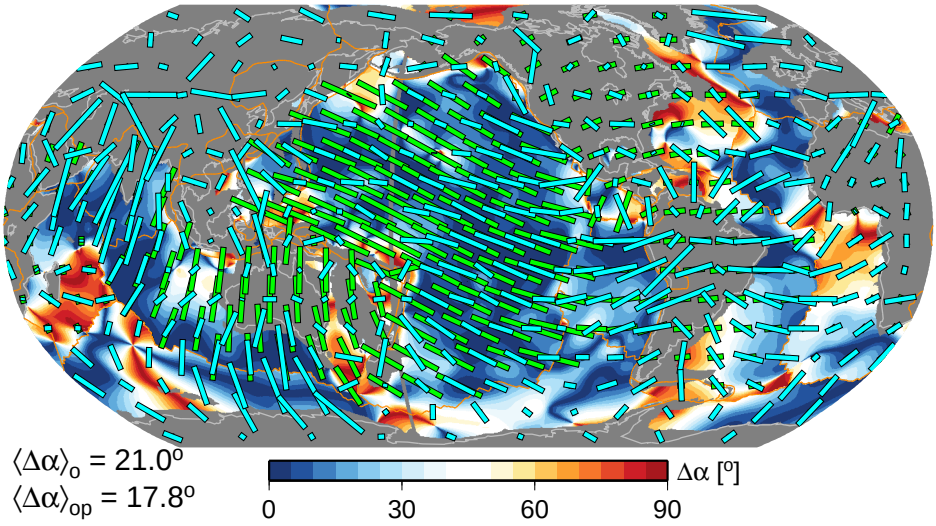


**Figure S3**

***a) spread. align.***

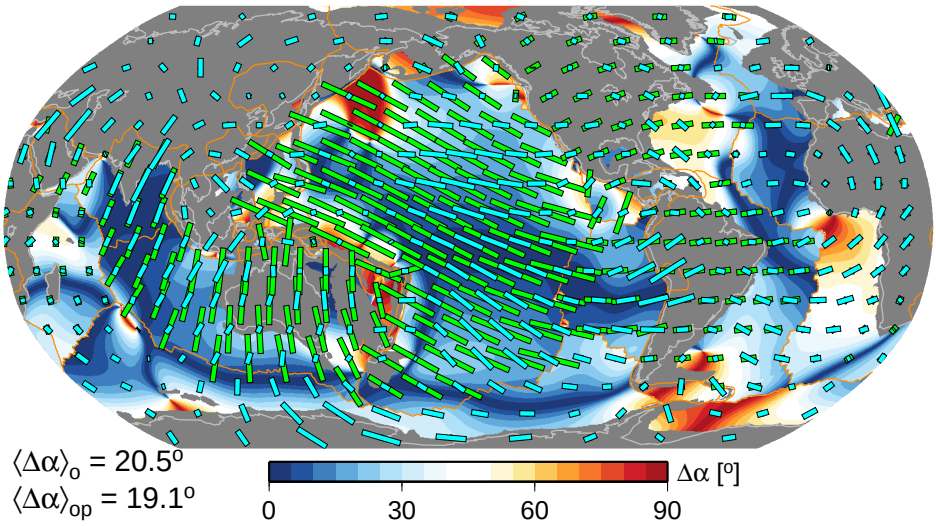


***b) YB13***

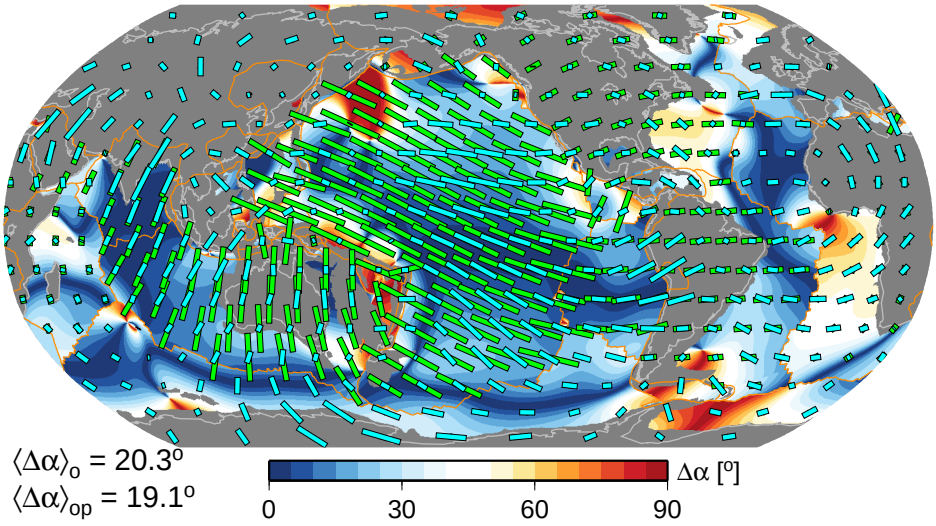


**Figure S4**